Malleability at the extreme nanoscale: Slow and fast quakes of few-body systems

Alireza Saffarzadeh[1,2,*] and George Kirczenow[2]

[1]*Department of Physics, Payame Noor University, P.O. Box 19395-3697, Tehran, Iran*

[2]*Department of Physics, Simon Fraser University, Burnaby, British Columbia, Canada V5A 1S6*

(Received 21 July 2017; revised manuscript received 20 October 2017; published 2 November 2017)

We explore the malleability of ultrasmall metal nanoparticles by means of *ab initio* calculations. It is revealed that, when strained, such nanoparticles exhibit complex behavior, including bifurcation between slow and fast quakes of their atomic structure, despite being few-body systems. We show the bifurcation to arise from the collapse of the nanoparticle's stiffness and a broken soft-mode symmetry, and that whether a slow or fast quake occurs can be controlled by varying the amplitude of the externally applied strains. We predict that while energy is released abruptly in a fast quake, surprisingly it continues to build up during a slow quake, and that, in common with slow-slip geological earthquakes, the slow nanoparticle quake is a silent precursor to a fast "seismic" quake. We show that electrical conductance and force measurements can detect and distinguish between slow and fast quakes, opening the way for experiments and potential applications of these phenomena.

DOI: 10.1103/PhysRevB.96.195403

I. INTRODUCTION

The malleability of metals, i.e., their ability to deform plastically without fracturing, has been exploited since prehistoric times in the making of ornaments, tools, and weapons. It continues to have numerous practical applications today, and the study of plasticity, shear, and fracture of macroscopic matter is an active area of research [1–10]. However, little, if anything, is known at present, either experimentally or theoretically, regarding the malleability of nanoparticles, despite its potential importance and the long-standing, intense interest in the physics of nanoparticles, including their structural [11–13], electronic [14–16], optical [17,18], plasmonic [18,19], magnetic [20,21], thermal [12], and transport [14,15,20] properties. Here we explore the malleability of ultrasmall (<1 nm) metal nanoparticles theoretically by means of first-principles computer simulations of the deformation of copper atomic clusters, as may be realized in a mechanically controlled break junction or scanning tunneling microscope setup. We establish that these nanoparticles exhibit malleability as distinct from brittleness. We find that under uniaxial elongation or compression, the nanoparticle normally deforms gradually, at first elastically and then plastically. However, these gradual deformations are punctuated by sudden events that we will refer to as "quakes." During quakes, some of the interatomic separations switch rapidly between values typical of nearest-neighbor and second-neighbor distances. Given the seeming simplicity of the few-atom nanoparticles that we consider, the behavior of the quakes is revealed by the present investigation to be surprisingly complex and interesting. We find quakes of two different types: (i) Fast quakes in which the atomic configuration changes abruptly and the total energy of the nanoparticle *decreases discontinuously*, and (ii) slow quakes in which the atomic configuration changes in a series of closely spaced smaller steps while, unexpectedly, the total energy *increases* smoothly. We predict bifurcation to occur between slow and fast quakes due to the collapse of the nanoparticle's stiffness and breaking of a symmetry associated with soft vibrational modes. We demonstrate that we are able to *control* whether a slow or fast quake occurs by choosing the *amplitude* of the forcing uniaxial strain applied to the nanoparticle. We find that the slow and fast quakes result in differing atomic configurations of the nanoparticle, and that a slow quake acts as a *precursor* to a subsequent fast quake that results in yet a third atomic configuration. We also show that conductance and force measurements can distinguish between fast and slow quakes. The behavior of the slow and fast quakes that we have discovered in few-atom nanoparticles has surprising commonalities with geological subduction zone earthquakes. Namely, in common with our findings for nanoparticle quakes, it has been suggested that some violent (fast) earthquakes follow silent slow-slip precursor earthquakes [22,23], and that whether a geological fault alternates between slipping slowly (silently) and fast (seismically) depends on the loading conditions [24]. However, in contrast to a recent proposal regarding geological earthquakes [24], we find the reduced stiffness signaled by the onset of a soft mode to play a crucial role in slow nanoparticle quakes.

II. METHODOLOGY

In the remainder of this paper, we elucidate these remarkable findings by presenting representative results for nanoparticles consisting of eight copper atoms. The atomic positions and interatomic distances were estimated by minimizing the total energy of the system, computed within density functional theory using the GAUSSIAN 09 package with the PBE1PBE functional and Lanl2DZ pseudopotentials and basis sets [25,26]. In all optimized geometries, the electronic energy and ionic forces were converged within 10^{-5} eV and 0.0008 eV/Å, respectively.

Initially, the structure was optimized without any constraint to find the minimum energy E_0, the corresponding arrangement of the copper atoms, and the distances d_{ij} between atoms i and j, $d_{ij} = |\mathbf{R}_j - \mathbf{R}_i|$. Here $\mathbf{R}_i$ is the position of atom i. The lowest-energy structure [shown in (a) of Fig. 1] was found

*Author to whom correspondence should be addressed: asaffarz@sfu.ca

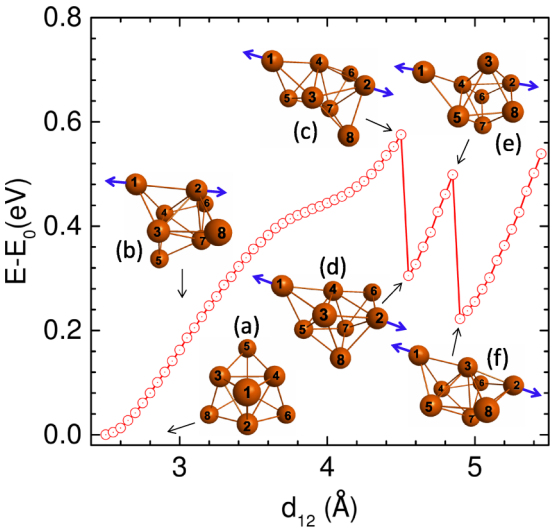

FIG. 1. Variation of the total energy of the eight-atom copper cluster during stretching of the interatomic distance d_{12}. (a) The lowest-energy geometry of the unconstrained cluster. (b)–(f) Atomic arrangements of the cluster for different stretching lengths d_{12} [27]. Blue arrows mark atoms 1 and 2 and show the direction of elongation for each structure. Black arrows indicate the corresponding d_{12} values. The lines are guides to the eye. Energies are measured relative to the lowest-energy E_0 of the unstrained nanoparticle.

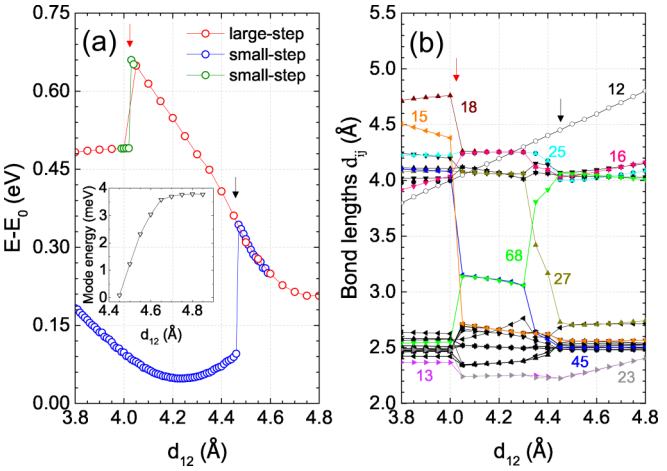

FIG. 2. (a) Total energy of the copper cluster during compression of d_{12} by steps of 0.01 Å (blue and green circles) and 0.05 Å (red circles). Inset: Energy of the soft vibrational mode approaches zero for $d_{12} \sim 4.45$ Å where both fast and slow quakes begin. (b) Bond lengths d_{ij} (labeled ij) plotted vs d_{12} for 0.05 Å compression steps. Most d_{12} values cluster around first- and second-neighbor distances. In both (a) and (b), red (black) arrows indicate where only fast (both fast and slow) quake(s) occur. Lines are guides to the eye.

to have tetrahedral symmetry, i.e., the point group T_d. Its first-, second-, and third-neighbor atomic distances were found to be 2.48, 4.08, and 4.12 Å, respectively.

Starting from this minimum energy structure, the nanoparticle was strained as follows: A pair of atoms i and j was chosen, and their separation d_{ij} was increased by 0.05 Å. Then atoms i and j were frozen and the other atoms of the nanoparticle were allowed to relax so as to minimize the total energy. This elongation of d_{ij} and energy optimization were repeated multiple times. Our results, obtained by increasing the distance between atoms 1 and 2, d_{12}, stepwise in this way are presented in Fig. 1. Qualitatively similar behavior was found if other atoms were chosen instead of 1 and 2.

III. RESULTS AND DISCUSSION

Figure 1 shows how the total energy of the nanoparticle changes as the cluster is stretched in this way, and also how the nanoparticle's geometry evolves in this process. Stretching the copper cluster initially increases the total energy in a parabola-like way due to the quadratic effective interatomic potential for small atomic displacements from their equilibrium positions. In this regime, Hooke's law is obeyed and thus the deformation is elastic. However, as the cluster is stretched further from configuration (a) to configuration (b), the behavior evolves continuously from elastic to plastic deformation as the total energy characteristic changes from parabolic for small displacements (elastic deformation) to approximately linear behavior (plastic deformation). In the plastic regime, the bond between atoms 1 and 2 slowly ruptures, and this manifests itself as an inflection point in the energy. As the deformation increases further, another inflection point appears due to a new bond gradually forming between atoms 1 and 5 as the cluster evolves from structure (b) to (c).

Although plastic deformation of the cluster due to changes in the bonding topology occurs as d_{12} is stretched between configurations (a) and (c) in Fig. 1, both the total energy and all of the interatomic distances evolve smoothly and slowly throughout this process. In other words, substantial changes in these quantities occur gradually as d_{12} changes by $\sim$1 Å. By contrast, the transitions between configurations (c) and (d) and between (e) and (f) in Fig. 1 involve abrupt decreases in the total energy due to the sudden formation of new bonds. These events are examples of "fast quakes." They arise from instabilities built up in the system. In the transition from (c) to (d), a new bond forms abruptly between atoms 8 and 5, increasing the coordination numbers of atoms 8 and 5 and thus lowering the total energy. Similarly, in the transition from (e) to (f), new bonds form between atom 3 and atoms 1, 6, and 7, lowering the total energy abruptly. These results show that metal nanoparticles with dimensions as small as two times the nearest-neighbor distance can exhibit malleable behavior as distinct from brittle fracture.

In Fig. 2 we show the behavior of the nanoparticle if after stretching it (as in Fig. 1) we compress it by reducing the separation d_{12} in similar steps, again freezing the positions of atoms 1 and 2 and allowing the other atoms to relax after each step. The starting geometry for compressing the cluster is the stretched structure with $d_{12} = 5.45$ Å. In Fig. 2(a) the total energy of the cluster is shown in red, blue, and green for d_{12} compressed in larger and smaller steps, 0.05, 0.01, and 0.01 Å, respectively.

Comparing Fig. 2(a) with Fig. 1, it is evident that the deformations of the cluster are not reversible. In particular, for elongation of d_{12} in 0.05 Å steps, the cluster exhibits two fast quakes at $d_{12} = 4.55$ and 4.9 Å, as shown in Fig. 1.

By contrast, under compression, for the 0.05 Å d_{12} step size [red circles in Fig. 2(a)] there is instead one fast quake at $d_{12} = 4$ Å indicated by the red arrow.

However, surprisingly, for compression of d_{12} by smaller 0.01 Å steps [blue circles in Fig. 2(a)], a fast quake appears in the total energy at $d_{12} = 4.45$ Å indicated by the black arrow, whereas no feature is evident in the energy for d_{12} values in that vicinity for the larger 0.05 Å d_{12} compression steps [red circles in Fig. 2(a)].

To help understand this intriguing anomaly, we plot all of the interatomic distances d_{ij} of the nanoparticle against d_{12} for the larger 0.05 Å d_{12} compression steps in Fig. 2(b). Notice that, at the same value of $d_{12} = 4.45$ Å (indicated by the black arrow) where the "anomalous" fast quake for small steps occurs in Fig. 2(a), in Fig. 2(b) the values of d_{27} and d_{68} begin to change. After three 0.05 Å d_{12} steps, d_{27} has switched from a first-neighbor value near 2.7 Å to a second-neighbor value near 4 Å, whereas d_{68} has switched by a comparable amount in the opposite direction. Because these large (1 Å or greater) changes in the interparticle distances (d_{27} and d_{68}) occur during a small (0.15 Å) change in the forcing strain applied to d_{12}, this behavior constitutes a quake. But in contrast to fast quakes that occur within a single d_{12} step, this quake is spread over multiple steps. We therefore refer to it as a "slow quake." Furthermore, interestingly, unlike for fast quakes in which the total energy *drops* abruptly, in the slow quake the total energy continues to *rise* almost linearly while d_{12} changes, as is shown by the red circles near the black arrow in Fig. 2(a).

It is not a coincidence that this slow quake in Fig. 2(b) and the fast quake marked by the black arrow in Fig. 2(a) *both* begin at the same value 4.45 Å of d_{12}. It points to interesting physics that will be explained below.

Figure 3(a) shows the structure of the nanoparticle just before these slow and fast quakes begin, while the structures immediately after the slow and fast quakes are shown in Figs. 3(b) and 3(c), respectively. Comparing these pictures, it is clear that in the slow and fast quakes, the atoms of the nanoparticles are displaced in opposite directions. For example, after the slow quake [Fig. 3(b)], atom 3 is lower than in the prequake structure [Fig. 3(a)], whereas after the fast quake [Fig. 3(c)] the same atom 3 is higher. In each case, the other atoms of the nanoparticle (apart from the forcing atoms 1 and 2) have moved in roughly the same direction as atom 3.

The physical reason for this symmetry between the atomic displacements of the slow and fast quakes can be understood by considering the vibrational normal modes of the copper nanoparticle with atoms 1 and 2 frozen. The calculated vibron energy for one of those modes is shown as a function of d_{12} in the inset of Fig. 2(a). It is evident that this is a soft mode whose frequency approaches zero near $d_{12} = 4.45$ Å where the slow and fast quakes both begin. The normalized atomic displacements in the soft mode are shown as red arrows in Figs. 3(d) and 3(e) for the nanoparticle geometries immediately preceding the slow and fast quakes. The atomic displacements shown in Figs. 3(d) and 3(e) clearly belong to the same soft mode; they differ only in that they are phase-shifted by π relative to each other.

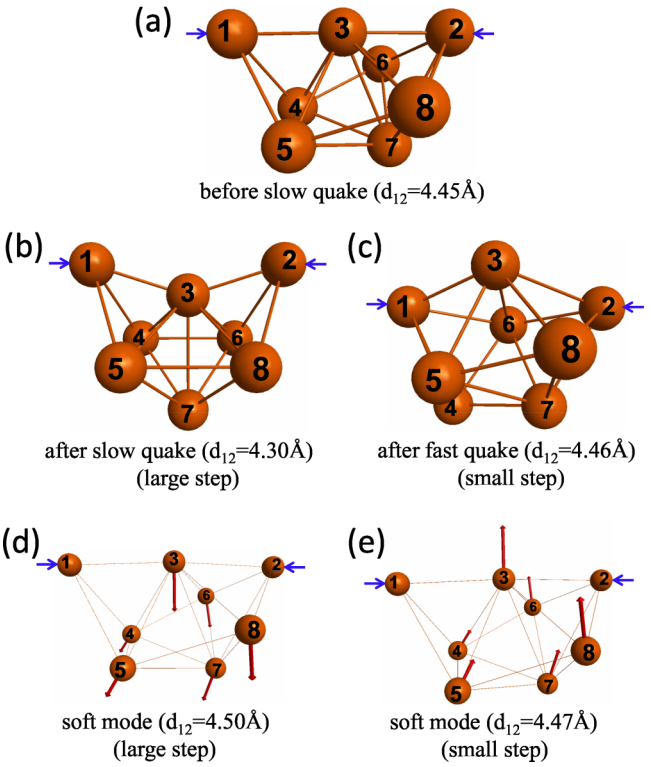

FIG. 3. Atomic arrangements of the copper nanoparticle [27] for compression along d_{12} (a) before and (b) after slow quake, and (c) after fast quake. (d) and (e) Atomic arrangements and soft mode (red vectors) during compression by large and small steps, respectively. The blue arrows show the direction of d_{12} compression in each structure.

Most importantly, the atomic displacements that happen in the slow and fast quakes [Figs. 3(b) and 3(c)] are strikingly similar to the soft-mode atomic displacements shown in Figs. 3(d) and 3(e), respectively. We conclude that these slow and fast quakes both occur because the stiffness of the nanoparticle against the soft-mode-like atomic displacements [shown in Figs. 3(d) and 3(e)] collapses when the soft-mode frequency approaches zero for $d_{12} \sim 4.45$ Å. In the harmonic approximation, *small* atomic displacements in the opposite directions shown in Figs. 3(d) and 3(e) require equal amounts of energy. However, for the large displacements that occur in the fast and slow quakes, this symmetry is broken by anharmonicity. In addition, the slow-quake-type displacements [Figs. 3(b) and 3(d)] cost additional energy, whereas for fast-quake-type displacements [Figs. 3(c) and 3(e)] the total energy of the nanoparticle decreases spontaneously. This difference in the energetics between the fast and slow quakes is evident from the different behavior of the red (slow quake) and blue (fast quake) energy plots in Fig. 2(a) as d_{12} decreases below 4.45 Å as marked by the black arrow. Compression of d_{12} by larger (smaller) 0.05 Å (0.01 Å) steps supplies more (less) energy to the nanoparticle. Thus the larger compression steps result in the slow quake in which the total energy increases, while the smaller steps result in the fast quake in which the total energy decreases. Thus we can *control* whether a slow or fast quake happens by choosing the amplitude of the

forcing strains applied to d_{12}. In other words, this demonstrates that if we squeeze a nanostructure gradually, we can get a very different result than by applying larger abrupt strains akin to hammering it. Both cases are physical, with different ways of compressing the structure producing different results. Here we have assumed that the abrupt compression of d_{12} is fast compared to the equilibration time of the nanoparticle structure. It is reasonable to expect the equilibration to become slower at lower temperatures and also as the soft-mode frequency approaches zero.

Another important feature of Fig. 2(a) is that if the nanoparticle continues to be compressed after the slow quake has occurred, the total energy of the system continues to build almost linearly until the fast quake indicated by the red arrow occurs. That is, the slow quake acts as a precursor to this fast quake. [Reducing the step size does not alter the nature of this subsequent fast quake, as can be seen by comparing the red and green circles in Fig. 2(a).] We note that since there is no release of energy during a slow quake (the total energy continues to grow during the slow quake), the slow quake should be regarded as "silent," as is the case for slow geological earthquakes [22–24]. It should also be noted that we found qualitatively similar behavior of fast and slow quakes and their relationships as well as similar underlying physics if instead of d_{12} we stretched and compressed other interparticle distances d_{ij} in similar ways.

Since quakes alter the structure of the nanoparticle, the total energy and related, potentially experimentally accessible, physical properties such as electronic conductance and the applied force required for a mechanical deformation can be affected strongly.

To investigate the effect of quakes on electronic transport through the nanoparticle, we calculated the electron transmission probabilities T through the cluster at the Fermi energy ϵ_F of the macroscopic electrodes used in conductance measurements. These, within Landauer theory [28], are related to the conductance via $g(\epsilon_F) = g_0 T(\epsilon_F)$, where $g_0 = 2e^2/h$ is the conductance quantum. Here, $T = \sum_{\alpha,\beta} |t_{\beta\alpha}|^2 \frac{v_\beta}{v_\alpha}$, $t_{\beta\alpha}$ is the transmission amplitude through the cluster, and α (β) is the electronic state of a carrier with velocity v_α (v_β) in the source (drain) lead. The leads are attached to the two copper atoms that are under compression, with separation d_{ij}. Figure 4(a) shows how the conductance at the Fermi energy, $g(\epsilon_F)$, evolves during compression by small and large steps, versus parameter d_{12}. The slow quake results in a large (factor ~2) smooth decrease in conductance, while fast quakes appear as abrupt, small conductance steps. The large conductance decrease during the slow quake can be understood intuitively as a result of the less compact structure after the slow quake [compare Figs. 3(b) with Figs. 3(a) and 3(c)], which also accounts for the *increase* in the total energy of the nanoparticle during the slow quake in Fig. 2(a).

The mechanical force, F_m, during compression of the copper cluster can be calculated from the numerical derivative of the total energy with respect to the length parameter d_{12} using the equation $F_m(d_{12,i}) = -[E(d_{12,i+1}) - E(d_{12,i})]/\delta_i$, where $d_{12,i}$ is the length parameter of compression step i, $E(d_{12,i})$ is the total energy in terms of $d_{12,i}$, and $\delta_i = d_{12,i+1} - d_{12,i}$.

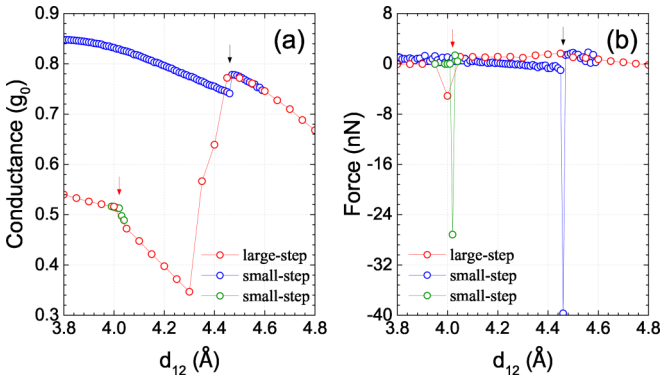

FIG. 4. (a) Calculated conductance and (b) the mechanical force required to compress the cluster when the distance d_{12} is compressed by small (blue and green circles) and large (red circles) steps. The arrows indicate the d_{12} values at which the slow and fast quakes appear; their colors and locations are as in Fig. 2. The lines are guides to the eye.

We have depicted in Fig. 4(b) the magnitude of the force versus parameter d_{12} for small-step and large-step compressions. The force shows a strong spike whenever a fast quake occurs because the total energy decreases abruptly, but no comparable feature is displayed for a slow quake.

Therefore, as can be seen in Figs. 4(a) and 4(b), the conductance and force together can in principle distinguish between slow and fast quakes experimentally. Hence, in addition to being of fundamental interest, experimental studies of malleability at the nanoscale based on these findings may be relevant for nanoelectronic applications.

IV. CONCLUSIONS

In summary, our investigation has established theoretically that ultrasmall metal nanoparticles are malleable, and it has revealed surprising bifurcatory behavior of the response of nanoparticles to externally applied strains. The bifurcation arises from anharmonicity breaking of the inversion symmetry of a soft vibrational mode of the nanoparticle. It manifests as slow and fast quakes that alter the structure of the nanoparticle. We have shown that whether a slow or fast quake occurs can be controlled by varying the amplitude of the applied strain. We have also shown that energy is released abruptly in a fast quake, but, by contrast, it continues to build up during a slow quake. In common with slow-slip geological earthquakes, we predict that the slow nanoparticle quake will be a silent precursor of a fast "seismic" quake. We have shown that electrical conductance and force measurements can detect and distinguish between slow and fast quakes, opening the way to experiments and potential applications of this interesting phenomenon.

ACKNOWLEDGMENTS

This work was supported by NSERC, CIFAR, WestGrid, and Compute Canada.

[1] C.-H. Chen, E. Bouchbinder, and A. Karma, Instability in dynamic fracture and the failure of the classical theory of cracks, Nat. Phys. (2017), doi: 10.1038/nphys4237.

[2] D. V. Denisov, K. A. Lörincz, J. T. Uhl, K. A. Dahmen, and P. Schall, Universality of slip avalanches in flowing granular matter, Nat. Commun. **7**, 10641 (2016).

[3] J. Barós, M. L. Hattali, D. Dalmas, and D. Bonamy, Fluctuations of Global Energy Release and Crackling in Nominally Brittle Heterogeneous Fracture, Phys. Rev. Lett. **113**, 264301 (2014).

[4] J. Barós, L. Barbier, and D. Bonamy, Crackling Versus Continuumlike Dynamics in Brittle Failure, Phys. Rev. Lett. **111**, 054301 (2013).

[5] M. Grob, J. Schmittbuhl, R. Toussaint, L. Rivera, S. Santucci, and K. J. Måløy, Quake catalogs from an optical monitoring of an interfacial crack propagation, Pure Appl. Geophys. **166**, 777 (2009).

[6] D. Bonamy, Intermittency and roughening in the failure of brittle heterogeneous materials, J. Phys. D **42**, 214014 (2009).

[7] J. S. Langer, Shear-transformation-zone theory of plastic deformation near the glass transition, Phys. Rev. E **77**, 021502 (2008).

[8] K. J. Måløy, S. Santucci, J. Schmittbuhl, and R. Toussaint, Local Waiting Time Fluctuations Along a Randomly Pinned Crack Front, Phys. Rev. Lett. **96**, 045501 (2006).

[9] M. L. Falk and J. S. Langer, Dynamics of viscoplastic deformation in amorphous solids, Phys. Rev. E **57**, 7192 (1998).

[10] M. L. Falk, M. Toiya, and W. Losert, Shear transformation zone analysis of shear reversal during granular flow, arXiv:0802.1752.

[11] C. L. Johnson, E. Snoeck, M. Ezcurdia, B. Rodríguez-González, I. Pastoriza-Santos, L. M. Liz-Marzán, and M. J. Hÿtch, Effects of elastic anisotropy on strain distributions in decahedral gold nanoparticles, Nat. Mater. **7**, 120 (2007).

[12] C. Hock, C. Bartels, S. Straßburg, M. Schmidt, H. Haberland, B. von Issendorff, and A. Aguado, Premelting and Postmelting in Clusters, Phys. Rev. Lett. **102**, 043401 (2009).

[13] C.-C. Chen, C. Zhu, E. R. White, C.-Y. Chiu, M. C. Scott, B. C. Regan, L. D. Marks, Y. Huang, and J. Miao, Three-dimensional imaging of dislocations in a nanoparticle at atomic resolution, Nature (London) **496**, 74 (2013).

[14] D. C. Ralph, C. T. Black, and M. Tinkham, Spectroscopic Measurements of Discrete Electronic States in Single Metal Particles, Phys. Rev. Lett. **74**, 3241 (1995).

[15] O. Agam, N. S. Wingreen, B. L. Altshuler, D. C. Ralph, and M. Tinkham, Chaos, Interactions, and Nonequilibrium Effects in the Tunneling Resonance Spectra of Ultrasmall Metallic Particles, Phys. Rev. Lett. **78**, 1956 (1997).

[16] Y. Lykhach, S. M. Kozlov, T. Skála, A. Tovt, V. Stetsovych, N. Tsud, F. Dvořák, V. Johánek, A. Neitzel, J. Mysliveček, S. Fabris, V. Matolín, K. M. Neyman, and J. Libuda, Counting electrons on supported nanoparticles, Nat. Mater. **15**, 284 (2016).

[17] J. Zheng, C. Zhang, and R. M. Dickson, Highly Fluorescent, Water-Soluble, Size-Tunable Gold Quantum Dots, Phys. Rev. Lett. **93**, 077402 (2004).

[18] M. Barbry, P. Koval, F. Marchesin, R. Esteban, A. G. Borisov, J. Aizpurua, and D. Sánchez-Portal, Atomistic near-field nanoplasmonics: Reaching atomic-scale resolution in nanooptics, Nano Lett. **15**, 3410 (2015).

[19] J. A. Scholl, A. L. Koh, and J. A. Dionne, Quantum plasmon resonances of individual metallic nanoparticles, Nature (London) **483**, 421 (2012).

[20] M. M. Deshmukh, S. Kleff, S. Guéron, E. Bonet, A. N. Pasupathy, J. von Delft, and D. C. Ralph, Magnetic Anisotropy Variations and Nonequilibrium Tunneling in a Cobalt Nanoparticle, Phys. Rev. Lett. **87**, 226801 (2001).

[21] P. N. Hai, S. Ohya, and M. Tanaka, Long spin-relaxation time in a single metal nanoparticle, Nat. Nanotechnol. **5**, 593 (2010).

[22] S. Y. Schwartz and J. M. Rokosky, Slow slip events and seismic tremor at circum-Pacific subduction zones, Rev. Geophys. **45**, RG3004 (2007).

[23] A. Socquet, J. P. Valdes, J. Jara, F. Cotton, A. Walpersdorf, N. Cotte, S. Specht, F. Ortega-Culaciati, D. Carrizo, and E. Norabuena, An 8 month slow slip event triggers progressive nucleation of the 2014 Chile megathrust, Geophys. Res. Lett. **44**, 4046 (2017).

[24] G. C. Mclaskey and F. Yamashita, Slow and fast ruptures on a laboratory fault controlled by loading characteristics, J. Geophys. Res. Solid Earth **122**, 3719 (2017).

[25] M. J. Frisch, G. W. Trucks, H. B. Schlegel, G. E. Scuseria, M. A. Robb, J. R. Cheeseman, G. Scalmani, V. Barone, B. Mennucci, G. A. Petersson *et al.*, The GAUSSIAN 09 Revision: A.02 computer code was used.

[26] J. P. Perdew, K. Burke, and M. Ernzerhof, Generalized Gradient Approximation Made Simple, Phys. Rev. Lett. **77**, 3865 (1996).

[27] B. M. Bode and M. S. Gordon, MacMolPlt: a graphical user interface for GAMESS, J. Mol. Graph. Model. **16**, 133 (1998).

[28] S. Datta, *Electronic Transport in Mesoscopic Systems* (Cambridge University Press, Cambridge, 1995).